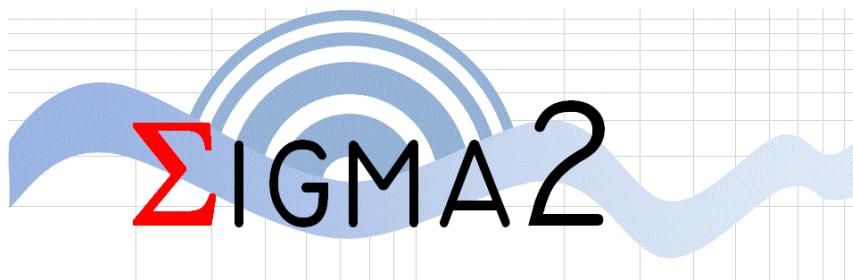
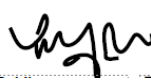



# Database of damage-consistent natural & synthetic seismograms

Work Package 6 "Ground-motion for engineers"



AUTHORS		REVIEW		APPROVAL	
Name	Date	Name	Date	Name	Date
Marco Fasan Matteo Barnaba	2020/10/30	Y. Bozorgnia  Y. Fukushima	22/8/22	 Public-access <input checked="" type="radio"/> SIGMA-2 restricted <input type="radio"/>	2023/01/13

## Document history

DATE	VERSION	COMMENTS
YYYY/MM/DD	0	

## Executive summary

The actual practice of seismic-risk assessment for critical infrastructures is based on Uniform Hazard Spectra (UHS) derived from Probabilistic Seismic Hazard Assessment (PSHA) in the format of (pseudo) spectral accelerations. The spectral (force-based) method is still widely applied in earthquake engineering, especially in the design of systems. It is also applied in fragility analysis. The UHS, and subsequently the time-histories derived based on it, has the problem that in reality it does not represent a uniform hazard but the weighted contribution of earthquakes leading to very different macroseismic intensities at the plant site. Similar problems arise also when using other hazard representations that do not account for the time evolution of the signals.

Macroseismic intensity represents a measure of the strength of an earthquake record inferred from observed damage. According to the European Macroseismic Scale (EMS), different signals characterized by the same macroseismic intensity should lead to the same mean observed damage on buildings with homogenous characteristics (vulnerability classes). At the same time, macroseismic intensity allows to consider the variability of the ground motion parameters associated with the same damage potential. Therefore, to perform non-linear time-history analyses with intensity-consistent sets of accelerograms means to subject the structures to the same damaging potential and to catch the variability on ground motion parameters. In other words, macroseismic intensity is used as an alternative to commonly used intensity measures (e.g. pga, spectral acceleration etc.) since it is a proxy that assumes damaging capacity.

In the present work a database of natural accelerograms (199) is constructed matching available ground motions and macroseismic data. To increment the availability of accelerograms a large database of physics-based simulated events is computed (115'200). The events are represented by three components broadband accelerograms accounting for different sources of variability. Using a relation proposed in the first deliverable of this task, an instrumental macroseismic intensity have been assigned to each simulated triplet of accelerograms. The relation investigates the mean kinematic ductility demand of the accelerograms on buildings having different strength and vibrational characteristics, and link it with the macroseismic intensity. The macroseismic intensity is therefore used to separate accelerograms in damage-consistent bins.

## Table of Contents

Document history.....	2
Executive summary .....	2
Table of Contents .....	3
1. Introduction.....	4
2. Database of damage-consistent natural accelerograms.....	5
3. Database of damage-consistent synthetic accelerograms .....	8
3.1. Simulation technique description.....	8
3.1.1. Source model.....	8
3.1.2. Wave propagation model.....	10
3.2. Modelling choices and database computation .....	10
3.2.1. Faults characteristics .....	11
3.2.2. Crustal model and site characteristics.....	13
3.3. Comparison of simulated data with GMPEs .....	15
3.4. Intensity assignment.....	18
4. Conclusions.....	22
5. Bibliography.....	23
APPENDIX 1 Characteristics of the modelled SDOF systems.....	25
APPENDIX 2 File name description for the physics-based database .....	29
APPENDIX 3 Files header .....	30

## 1. Introduction

Classical Performance Based Seismic Design (PBSD) and seismic-risk assessment is based on Probabilistic Seismic Hazard Assessment (PSHA) (Cornell 1968) using as representative ground motion intensity measure the spectral acceleration. This procedure leads to the definition of the Uniform Hazard Spectrum (UHS), that is, a response spectrum that shows at each vibrational period the spectral acceleration having a predefined probability of exceedance in a fixed period of time. UHS represents a weighted value due to the contribution of different earthquakes having different damaging potential (Klügel and Stäuble-Akcaçay 2018), this is illustrated in a qualitative manner in Figure 1. Therefore, if a UHS is used as target spectrum, even when selecting spectrum compatible accelerograms, the final structural demands will be affected by the different damaging potential of each selected accelerogram; hence the structures under analysis are not subject to a uniform hazard. Moreover, even if spectral acceleration represents an efficient intensity measure and other more realistic hazard representations could be used (such as the conditional mean spectrum – CMS instead of the UHS), it still represents a peak and summary value and cannot capture all the damaging features of the earthquake that depend on the time evolution (incl. duration) of the ground motion.

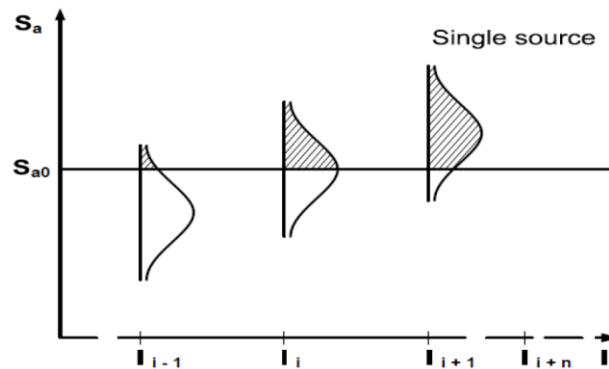


**Figure 1: Illustration of the calculation concept of PSHA (example for a single source that with different frequency can cause earthquakes of different strength leading to different site intensities).**

Seismic Hazard Assessment (either probabilistic or deterministic) can be done also using macroseismic intensity as intensity measure taking advantage of the longer duration of historical catalogues compared with instrumental ones. Differently from spectral acceleration, in principle macroseismic intensity represents a measure of the strength of the ground shaking inferred from the mean damage observed in a homogeneous area. In other words, buildings are used as sensors and the extent of damage is used as a measure of the strength of the signal. In particular, the European Macroseismic Scale - EMS (Grünthal 1998) should lead to consistent measures of the strength of the signal even if the built environment where the macroseismic intensity is assessed is very different. In other words, if the same earthquake (the same recorded signal) happens in two different cities with two different built environments, the evaluation of the intensity using the EMS should lead to the same value. This is assured subdividing buildings in different vulnerability classes and observed damage in different damage grades. Clearly, each step performed in the assignment of intensity introduces new uncertainties on the real intensity value. Uncertainties are mainly related to the subjectivity on the field definition of (Musson et al. 2010):

- vulnerability class of the building;
- damage grade reached by the building.

Since macroseismic intensity is directly based on observed damage, it follows that accelerograms having the same macroseismic intensity show the same damaging potential. Based on this consideration, non-linear time history analysis performed with accelerograms having the same

macroseismic intensity should lead, on average, to a damage consistent evaluation of the performance of a stock of buildings, therefore to a damage-consistent risk analysis.

As first part of this study, a methodology to assign the EMS macroseismic intensity ( $I_{EMS}$ ) to accelerograms was proposed using regression analysis on available data. The proposed methodology tries to simulate numerically the assignment procedure of macroseismic intensities on field and is based on regression equations between intensity and linear or non-linear ground motion parameters. Non-linear parameters are extracted from non-linear time history analysis using non-linear SDOF systems representative of the non-linear behaviour of different buildings vulnerability classes. Details of this analysis are reported in the first deliverable of this task (Fasan 2020).

In fact, few accelerograms are recorded directly inside areas where the macroseismic intensity is also evaluated. Hence, the possibility to assign the intensity to other recorded or simulated accelerograms can help to perform damage consistent risk assessments, increasing the number of available accelerograms to be used.

In order to increase the number of available accelerograms, this work focuses on the construction of a database of damage-consistent synthetic accelerograms. The damaging potential is evaluated using the macroseismic intensity as a proxy. The damage-consistency is therefore assured taking advantage of the relations produced in the first part of this task and described in the first deliverable (Fasan 2020).

The EMS scale is chosen since it is the reference macroseismic scale in Europe since 1998 and its vulnerability model is the most complete and updated. Nevertheless, the same procedure proposed here can be applied with any macroseismic scale.

The methodology is developed and proposed in the framework of the European project Seismic Ground Motion Assessment 2 (SIGMA-2, <http://www.sigma-2.net/>).

The final purpose of this database of damage-consistent natural and synthetic accelerograms is to be used to perform intensity-based fragility assessment and subsequent seismic risk analysis.

## 2. Database of damage-consistent natural accelerograms

This database represents the data used to develop the relations presented in Fasan (2020).

The procedure used to assemble the combined database of records and observed Macroseismic Intensity consisted in downloading the macrodata points (MDP) and the natural records from available databases and linking them using a maximum distance between the MDP and the record station.

The MDPs have been gathered mainly from the 2015 version of the Italian Macroseismic Database (DBMI) (Locati et al. 2016). The recorded accelerograms have been downloaded from the European Strong Motion Database (ESM) (Lanzano et al. 2019).

Data have also been integrated with publications available in literature. The following data have been used to integrate the MDPs available in DBMI:

- data of the 6 May 1976 Friuli earthquake were replaced with those available in Tertulliani et al. (2018) that re-evaluated the macroseismic intensity using the EMS and available surveys;
- data on MCS intensity of the 7 and 11 May 1984 central Italy earthquakes were replaced with those available in Graziani et al. (2017) defined in EMS intensity;
- replacing data of the 14 September 2003 Appennino Bolognese earthquake bases on information provided by the QUEST group (Quick Earthquake Survey Team);
- replacing data of the 6 April 2009 L'Aquila earthquake with those available in Azzaro et al. (2011);
- adding data of the 25 January 2012 Emilia earthquake available in Tertulliani et al. (2012);

- replacing data of the 21 June 2013 Lunigiana earthquake based on information provided by QUEST;
- adding data of the 2016 Central Italy earthquake sequence available in Arcoraci et al. (2019).

The final dataset consists in one-to-one data pairs (each MDP is linked with the closest record and the other way around) using a maximum distance of 3 km between the two points. The dataset is described in Table 1.

The records included in the final database and classified according to the macroseismic intensity are 199 derived from 31 different earthquakes. Moment magnitude ranges from 4.2 to 6.5. Figure 2 shows the magnitude vs epicentral distance distribution of the records included in the final dataset and the distribution of couples for each intensity degree arranged in bins with half-degree width. Macroseismic intensity ranges from  $I_{EMS}=III$  to  $I_{EMS}=XI$ . Figure 3 shows the distribution of the distances between the MDPs and the station and the distribution of magnitudes among the observed MDPs which is almost constant.

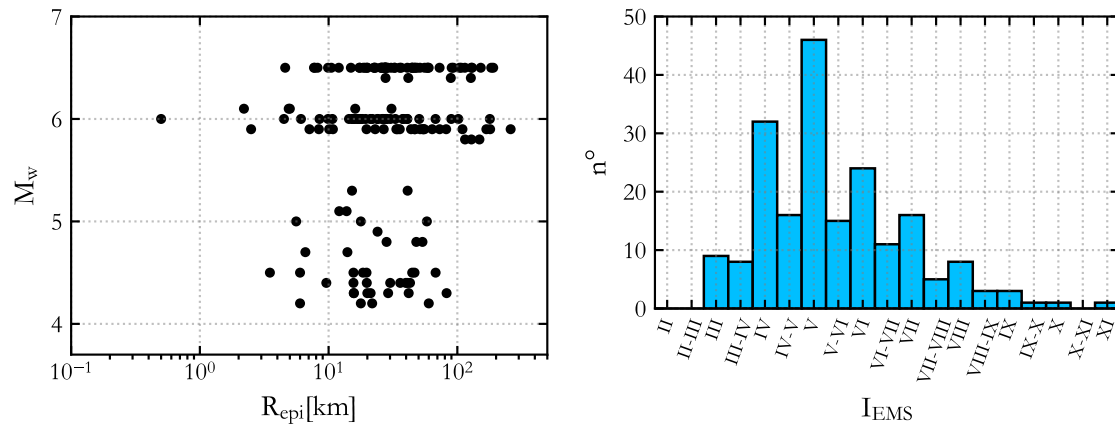


**Figure 2: Magnitude vs epicentral distance of the records included in the final dataset (left) and Distribution of couples MDP-record for each intensity degree (right)**

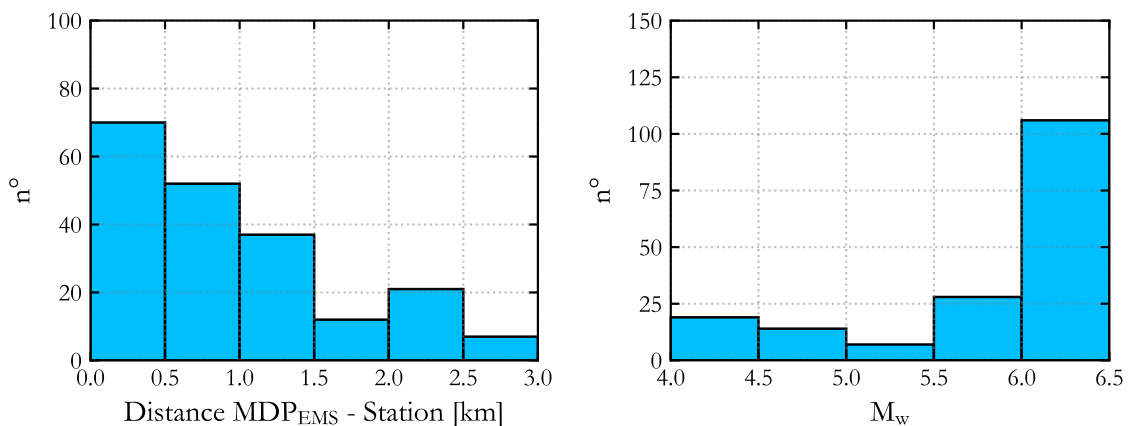


**Figure 3: Distribution of the distance MDP-station of the recorded the accelerogram (left) and Distribution of couples MDP-record for different magnitude ranges present in the final dataset (right)**

**Table 1: Characteristics of the final database with natural acclerograms**

ID	Date (dd/mm/yyyy)	Lat (°)	Lon (°)	Depth (km)	M <sub>w</sub>	M <sub>L</sub>	N° I-MDP
IT-1976-0002	06/05/1976	46.262	13.3	5.7	6.4	6.4	4
IT-1983-0004	20/07/1983	37.5487	15.168	24.7	4.5	4.3	1
IT-1984-0004	07/05/1984	41.7	13.86	20.5	5.9	5.9	10
IT-1999-0012	14/02/1999	38.183	15.019	12	4.7	3.9	1
IT-2001-0008	22/04/2001	37.702	15.02	5	4.2	3.2	1
IT-2002-0007	05/04/2002	38.352	15.096	5	4.4	4.2	1
IT-2002-0024	06/09/2002	38.381	13.701	5	5.8	5.6	3
IT-2002-0040	27/10/2002	37.76	15.116	5	4.9	4.8	1
IT-2003-0048	14/09/2003	44.255	11.38	8.3	5.3	5.0	2
IT-2006-0059	27/02/2006	38.155	15.2	9.2	4.4	4.1	6
IT-2006-0302	19/12/2006	37.778	14.913	23.8	4.2	4.1	2
IT-2009-0009	06/04/2009	42.342	13.38	8.3	6.1	5.9	4
IT-2009-0317	08/11/2009	37.847	14.557	7.6	4.4	4.4	1
IT-2009-0323	15/12/2009	43.007	12.271	8.8	4.2	4.3	1
IT-2009-0328	19/12/2009	37.782	14.974	26.9	nan	4.4	6
ISIDe-2166809	02/04/2010	37.799	15.079	0.3	nan	4.3	1
IT-2010-0032	16/08/2010	38.352	14.894	13.5	4.7	4.8	1
EMSC-20110506_0000042	06/05/2011	37.804	14.943	20.4	4.3	4.0	1
IT-2011-0110	23/06/2011	38.064	14.784	7.3	4.5	4.4	7
IT-2011-0020	17/07/2011	45.01	11.367	2.4	4.8	4.8	3
IT-2011-0022	25/07/2011	45.016	7.365	11	4.3	4.3	4
IT-2012-0002	25/01/2012	44.871	10.51	29	5.0	5.0	3
IT-2012-0008	20/05/2012	44.8955	11.2635	9.5	6.1	5.9	1
IT-2012-0011	29/05/2012	44.8417	11.0657	8.1	6.0	5.8	21
IT-2012-0061	25/10/2012	39.8747	16.0158	9.7	nan	5.0	13
IT-2013-0001	04/01/2013	37.881	14.719	9.6	4.3	4.4	2
IT-2013-0005	21/06/2013	44.1308	10.1357	7	5.1	5.2	2
IT-2013-0013	15/08/2013	38.111	14.913	19.4	nan	4.5	5
EMSC-20160824_0000006	24/08/2016	42.6983	13.2335	8.1	6.0	6.0	17
EMSC-20161026_0000095	26/10/2016	42.9087	13.1288	7.5	5.9	5.9	15
EMSC-20161030_0000029	30/10/2016	42.8322	13.1107	9.2	6.5	6.1	59

### 3. Database of damage-consistent synthetic accelerograms

In order to increase the availability of accelerograms and fill the gaps shown in the magnitude-distance distribution represented in Figure 2, in this section the construction of a database of damage-consistent physics-based synthetic accelerograms is presented. The work does not intend to simulate specific events that actually occurred but rather the shaking that could be recorded in the range of possible future events described in section 3.2.

#### 3.1. Simulation technique description

Ground motions are strongly influenced by the rupture process (e.g. nucleation point, rupture velocity, slip distribution, etc.), the direction of rupture propagation, and permanent ground displacements resulting from the fault slip. Other relevant factors influencing ground motions at a site of interest are represented by the characteristics of the crossed earth layers and by local site effects. These factors lead to high strong motion variability, in particular in the near fault zone and proper ground motion simulations need to reproduce them accurately.

In this work ground shaking is calculated through the tensor product between the tensors of the earthquake source and the Green's function of the medium (including the soil layers) crossed by the seismic waves (Magrin 2012; Panza et al. 2012; Fasan 2017). Seismic waves are modelled starting from the knowledge of the seismic sources and of the structural properties of the earth's lithosphere, allowing to take into account the kinematic complexity of the rupture process of the seismic source as well as site and path effects and, thus, considering the intra and inter-event spatial variability of the ground motion. The technique herein presented has been successfully applied and validated against past events and available ground motion prediction equations (Panza et al. 2012; Fasan et al. 2016; Magrin et al. 2016; Fasan 2017; Hassan et al. 2020).

In order to assess the ground shaking associated with the hypothesized seismic scenario, the calculation of synthetic accelerograms occurs in two phases:

1. simulation of the fault rupture process on the fault plane;
2. simulation of wave propagation and calculation of synthetic accelerograms for the sites of interest.

It is therefore necessary to model the properties of the seismic source and of the bedrock-soil structure interposed between the fault and the sites of interest.

##### 3.1.1. Source model

To calculate realistic accelerograms, in particular in the near fault zone, a finite-fault simulation is needed. An extended source (ES) model allows to catch the effects related to the kinematic rupture process (i.e. directivity) and, in the near field, to the dislocation (i.e. static displacement - fling step).

When the extended model is used, the source of the earthquake is considered a relative slip field distributed on the fault surface, on which the rupture process is presumed to occur. When modelling possible future seismic scenarios, no reasonable deterministic prediction for many details of a future fault motion can be expected. Therefore, the variability of the space and time evolution of the rupture can be treated in practice only from a statistical viewpoint. Correspondingly, in this work the simulation of the fault rupture is performed by the algorithm PULSYN through a Monte-Carlo approach as implemented by Gusev (Gusev 2011). The used method is a broadband kinematic stochastic simulation of the earthquake source. At low frequency the fault process is described deterministically, in terms of fault slip rate as a function of time and position on a fault. At higher frequencies (HF), which are mostly controlled by details of the propagating rupture, the fault process is treated in a stochastic manner.

The fault surface is then modelled as a grid of point sub-sources, whose seismic moment is calculated by considering each of them as a component of a realization of a non-stationary random process.



Assuming a realistic kinematic description of the rupture process, the extended seismic source model allows to generate a spectrum (in amplitude and phase) of the temporal function of the source that takes into account both the rupture process and the effects of directivity. For the chosen scenario, different possible realizations of the rupture process can be considered. Each realization is characterized by a different slip distribution on the fault plane, nucleation point and time evolution (see Figure 23). In this way the stochastic nature of the fault rupture is accounted for.

The simulation of the detailed space-time history of the source performed by the PULSYN algorithm can be briefly described as follows (Gusev 2011; Magrin 2012):

1. For a given moment magnitude  $M_w$ , the seismic moment value  $M_0$ , the length and width of the source rectangle, and mean rupture velocity (that defines the duration) are selected following average observed trends (Kanamori and Anderson 1975; Wells and Coppersmith 1994);
2. Step 1 guarantees that the low-frequency part of the source spectrum will have a realistic corner frequency, and that the far-field body-wave source signal will have realistic duration. Non-standard stress-drop values can be consistently accounted for. The simulated sub-sources are positioned in a grid pattern over the rectangle. Amplitudes of sub-sources are selected following a simulated distribution of the final slip. This 2D slip function is assumed to be a realization (sample function) of a 2D random process with an appropriate (power-law) power spectrum;
3. A predetermined nucleation/starting point ("hypocentre") within the rectangle is set, and the rupture front is assumed to propagate from this point, with a given velocity field for its kinematic simulation (e.g. unilateral, symmetric bilateral). The rupture front velocity is assumed to vary randomly along the distance from the hypocentre. The successive velocity values are randomly distributed, with predetermined mean and dispersion. The arrival of the front at a sub-source switches it on;
4. Each sub-source is assumed to slip (that is, to have non-zero slip velocity) only during its "active" time interval, with its duration comparable to the standard "rise time" parameter of Haskell-Aki-Heaton model (Haskell 1964; Aki 1967; Heaton 1990). The rise time is assumed to be similar in all points over the source rectangle and it is selected following Heaton's result that the width of the slipping part of the fault is approximately the 10% of its length. Thus, the rise time is set as a fraction (like 0.10) of the total rupture propagation time for the unilateral rupture case. To account for finiteness of sub-sources, this "ideal" rise time is then somewhat increased. The complete solution of the entire problem is reduced now to the construction of appropriate time functions of moment rate for each sub-source.
5. The "target" amplitude source spectrum is defined on the basis of a preferred theoretical or empirical spectral scaling law. The aim of the subsequent calculations is to construct a signal whose spectrum is close to the target one. Let us consider the "skeleton source", or the space-time object that consists of all white-noise sequences present in each sub-source. The far-field radiation of this source will have quite realistic spectral properties at low frequencies, because the general style of the space-time source behaviour and its numerical parameters are chosen to be realistic. At high frequencies (HF), however, the signal will be too rich in high frequency energy. To fit the HF part of the target spectrum, smoothing of the "skeleton" signal must be performed. A simple way to do such a smoothing is to convolve the white-noise sequences with a pulse of an appropriate shape. To determine such a shape function we compare the far-field amplitude spectral shape of the "skeleton" signal generated by the complete set of white-noise signals, on one side, and the realistic "target" amplitude spectral shape on the other side. Roughly speaking, the ratio of these spectra is calculated and then transformed to the time domain, yielding the appropriate pulse shape. The actual procedure is more complicated, since it includes the smoothing of the high-frequency part of the "skeleton" spectrum, and the accurate selection of the phase spectrum of the unit pulse. The resulting smoothing kernel represents a relatively short "unit pulse".

6. As a final step, for each sub-source its skeleton time history is shifted in time, by a delay corresponding to the rupture propagation kinematics, and then convolved with the common unit pulse, to produce the moment rate time function of this sub-source.

### 3.1.2. Wave propagation model

The seismograms calculation is conducted in laterally homogeneous media, i.e. the bedrock-soil structural model is represented by a semi-infinite space in plane and parallel inelastic layers, up to a frequency of 10 Hz and using two different techniques: the MS - modal summation technique (Panza 2001; Panza et al. 2012) and the DWN - discrete wavenumber technique in the implementation of Pavlov (Pavlov 2009). The modal summation technique (MS) is very fast and provide an accurate simulation of ground motion in far source condition, but it can be applied only when the epicentral distance is greater than the focal depth. The DWN gives the full wave field, including all body waves and near field and is applied when MS is not applicable. The limitation of maximum frequency to 10 Hz was selected as a compromise between accuracy of simulations, available information (in particular details of soil structure) and computational time. This aspect implies that these simulations should be applied only to structures where frequencies higher than 10Hz are not relevant in terms of producing damage or other relevant effects. If there was a need to apply them to such structures, their maximum frequency should be increased applying available techniques (e.g. Paolucci et al. 2018).

## 3.2. Modelling choices and database computation

As explained in previous sections, seismic ground motions are influenced by source, path and site effects. The combination of these effects makes it difficult, if even possible, to predict a priori the characteristics of an event showing a prefixed damage potential (here evaluated as a possible macroseismic intensity). Therefore, several possibilities need to be investigated in order to explore possible outcomes and build a database of damage-consistent ground motions. The main parameters herein considered are:

1. source focal mechanism;
2. moment magnitudes  $M_w$ ;
3. source rupture process (nucleation point, evolution of the front rupture, slip distribution, depth) treated as explained in Section 3.1.1;
4. characteristics of structure interposed between the source and the site of interest (path effects);
5. soil characteristic at the site of interest (site effects);
6. source-to-site distance  $R$ ;
7. angle between the source and the receiver at the site of interest.

The range of investigated values is shown in Table 2 and leads to a total of 115'200 different simulated events. The simulations workflow is shown Figure 4. Main characteristics of faults and soils are extracted from existing databases and described in Sections 3.2.1 and 3.2.2.

**Table 2: Range of investigated parameters**

Parameter	Range
Moment magnitude $M_w$	4.5 – 8.0, steps of 0.5
Distance $R$	5, 10, 15, 20, 40, 60, 80, 100 km
Local soil category	A, B, C (real stratigraphy, 5 each)
Receivers angles	6, 60° degrees increments
N° of different faults	4, with different focal mechanisms and deep soil structure (F1 to F4)

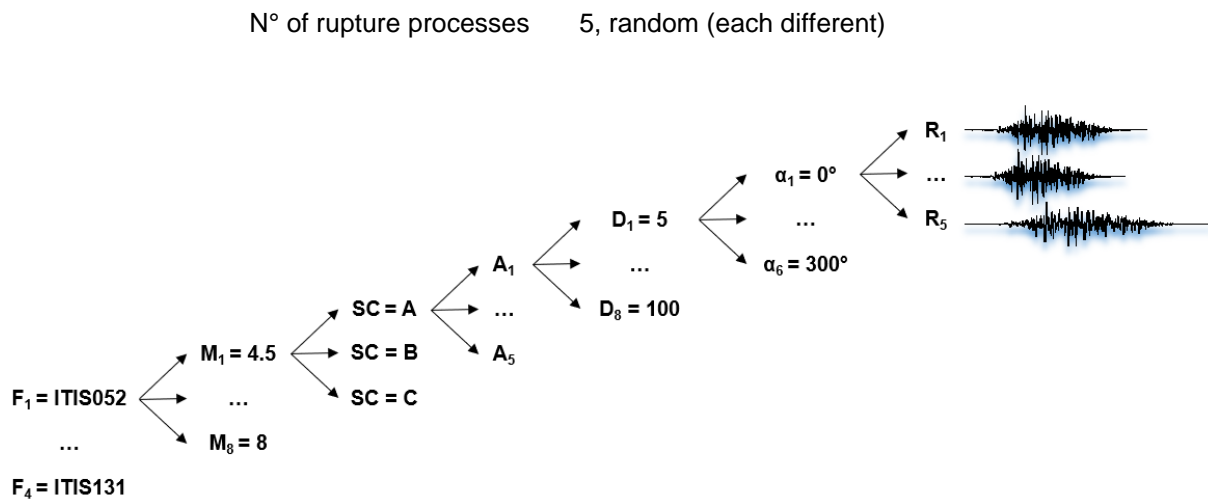


**Figure 4: Simulations workflow**

### 3.2.1. Faults characteristics

Faults main characteristics are extracted from the Database of Individual Seismogenic Sources compiled for Italy and surrounding areas (DISS Working Group 2018) and reported in Table 3. Four different faults have been considered in order to account for different focal mechanisms (normal, thrust or strike-slip faulting style) and geometrical features.

**Table 3: Main parameters of the modelled faults**

DISS-ID	ITIS052 (F4)	ITIS120 (F2)	ITIS107 (F3)	ITIS131 (F1)
<b>Name</b>	San Giuliano di Puglia	Gemona South	Mirandola	Paganica
<b>Faulting style</b>	Strike-slip	Thrust fault	Thrust fault	Normal Fault
<b>Location [Lat/Lon]</b>	41.69 / 14.94	46.25 / 13.14	44.85 / 11.07	42.32 / 13.45
<b>Length [km]</b>	10.5	16	9	14
<b>Width [km]</b>	8	9	5.9	9.5
<b>Min depth [km]</b>	12	2	4	3
<b>Strike [deg]</b>	267	290	108	133
<b>Dip [deg]</b>	82	30	30	43
<b>Rake [deg]</b>	203	105	90	275

Since several magnitudes are simulated, the fault area is chosen considering the scaling law for fault dimension according to Section 3.1.1. The fault minimum depth is selected according to Table 3. For each combination of fault, magnitude, local site stratigraphy, distance from the centre of the fault, and receiver angle, five different distributions of slips over the fault have been computed from a stochastic distribution leading a total of 115'200 different simulated earthquakes. The scaling laws proposed by Magrin et al. (2016) mainly for the Italian territory have been used as reference source spectrum. The average Mach parameter (ratio between rupture velocity and shear wave velocity) has been set to 0.8. Receivers have been placed at steps of 60° degrees according to the distances from the centre of the fault reported in Table 2. At the end of each simulation the event depth and epicentral distance have been set equal to those of the nucleation point. The horizontal projection of the considered faults (left) and the receivers arrangement (right) are shown from Figure 5 to Figure 8. In the pictures the rectangle represents the fault projection on the horizontal plane with the bold line identifying the top edge. The red

point represents the fault centre whereas the orange rectangle the area where the nucleation point may take place. Blue dots represent the sub-sources discretization. The figures on the right show the receiver positions with green triangles. The distances are reported in Table 2.

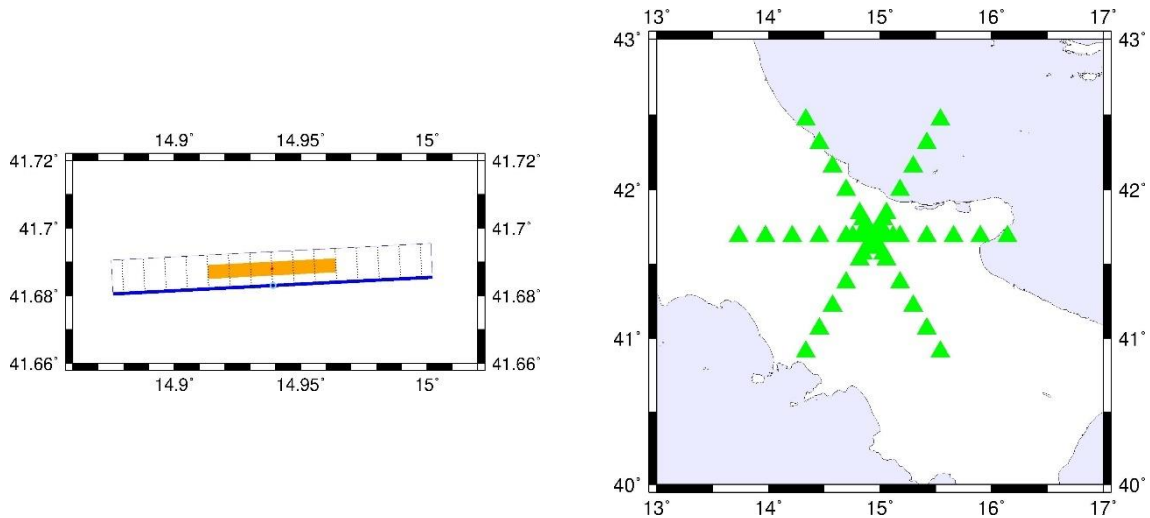


Figure 5: ITIS052 - San Giuliano di Puglia: fault projections and receivers arrangement

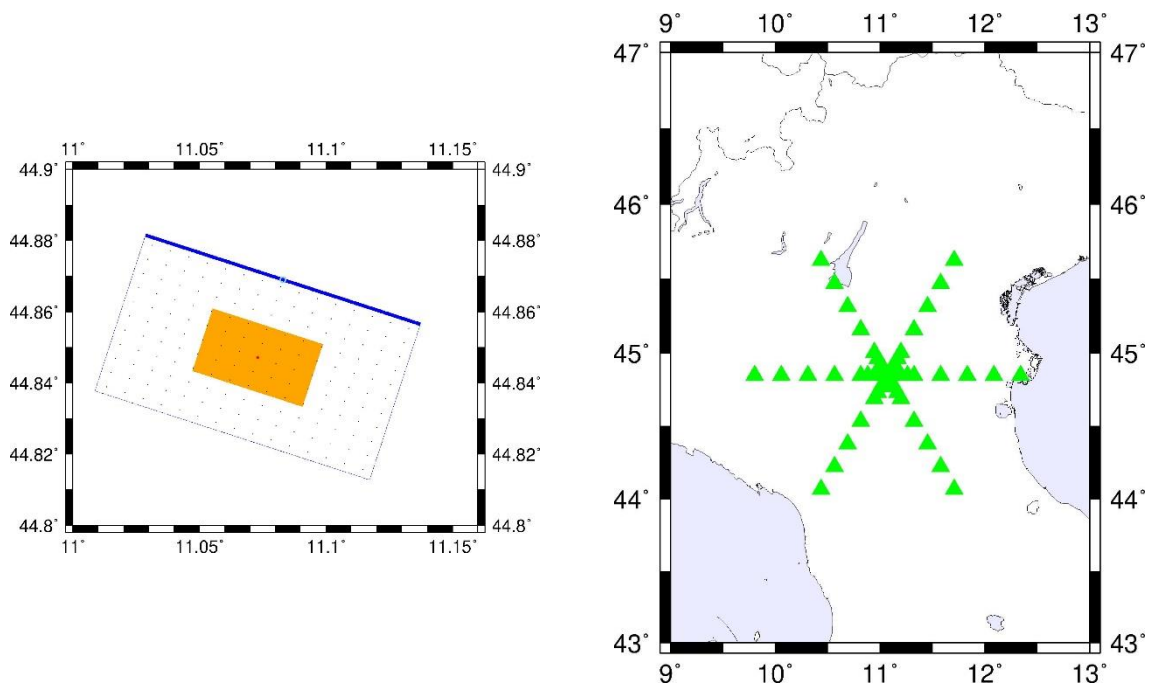
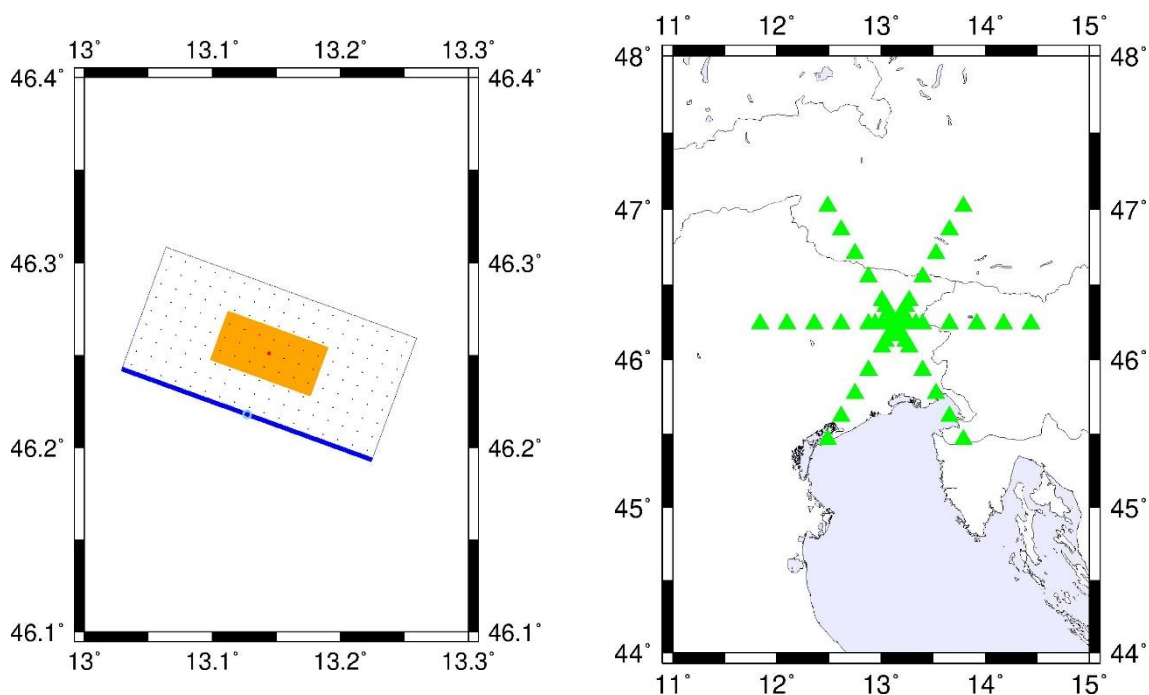
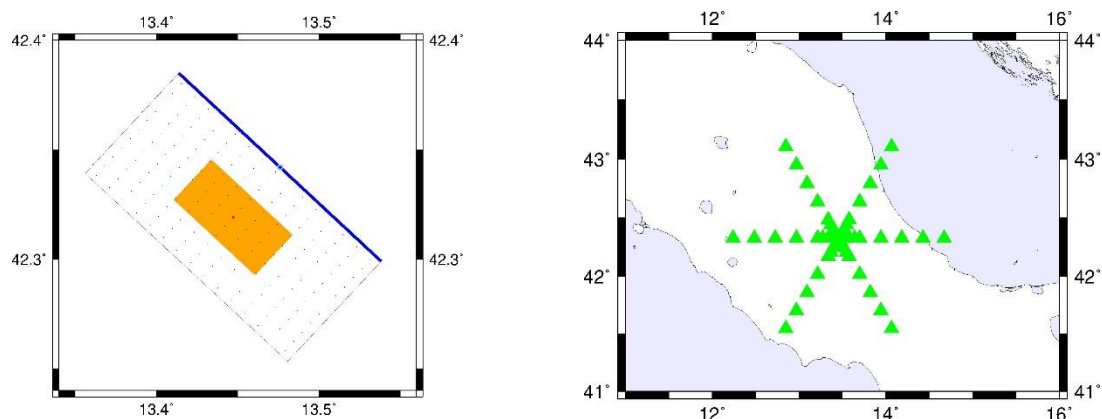


Figure 6: ITIS107 - Mirandola: fault projections and receivers arrangement



**Figure 7: ITIS120 – Gemona South: fault projections and receivers arrangement**



**Figure 8: ITIS131 – Paganica: fault projections and receivers arrangement**

### 3.2.2. Crustal model and site characteristics

Propagation modelling needs to account for path and site effects. The physical properties of the source-site paths are defined using a set of cellular structures obtained through an optimized nonlinear inversion of surface wave dispersion curves (Brandmayr et al. 2010). Each fault has been linked with a different deep structures representative of different Italian regions. Deep structures associated with each fault are shown in Figure 9 and Figure 10.

To account for local site effects, real site-specific soil layers have been placed above the deep structures. Soil category A, B and C according to Eurocode 8 classification have been considered (see Figure 11). For each fault and soil category five different shallow structures have been adopted, leading to a total of 60 different soil models (4 deep structures by 3 categories by 5 stratigraphy). The real stratigraphy have been downloaded from the European Strong Motion catalogue (Lanzano et al. 2019) and represent the characteristics of different recording stations. Among all those available, those that have the greatest depth of investigation were selected.

Selected structures are Italy-specific but coming from different regions and using different site-specific soil structures. We believe that signal differences between different European countries (related to deep soil structure) are not relevant compared to other source of variability such as site-specific soil or to uncertainties related to signal selection standard practice.

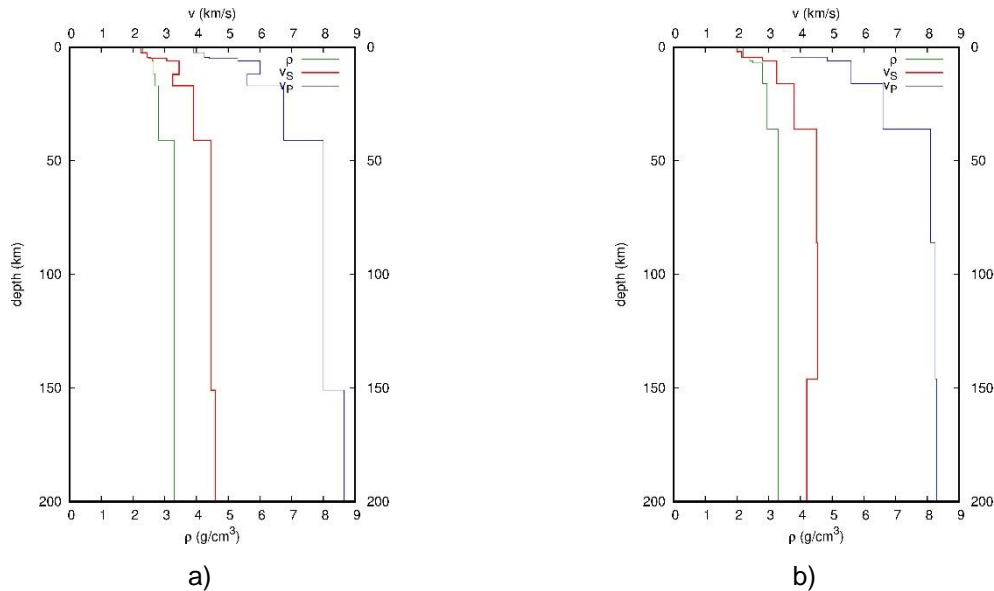


**Figure 9: Deep structures adopted for: a) ITIS052 - San Giuliano di Puglia and b) ITIS107 – Mirandola**

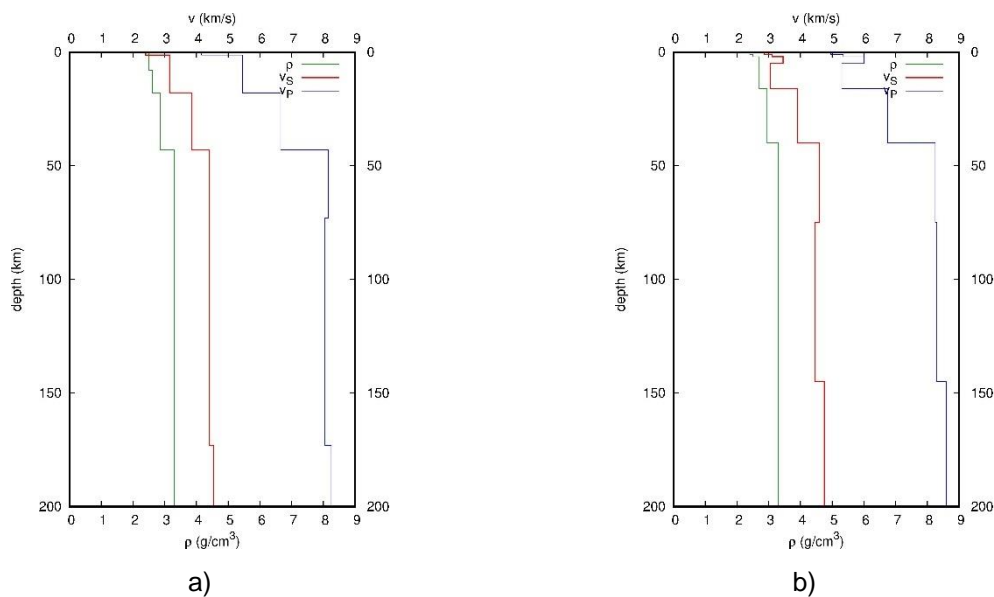


**Figure 10: Deep structures adopted for: a) ITIS120 – Gemona South and b) ITIS131 – Paganica**

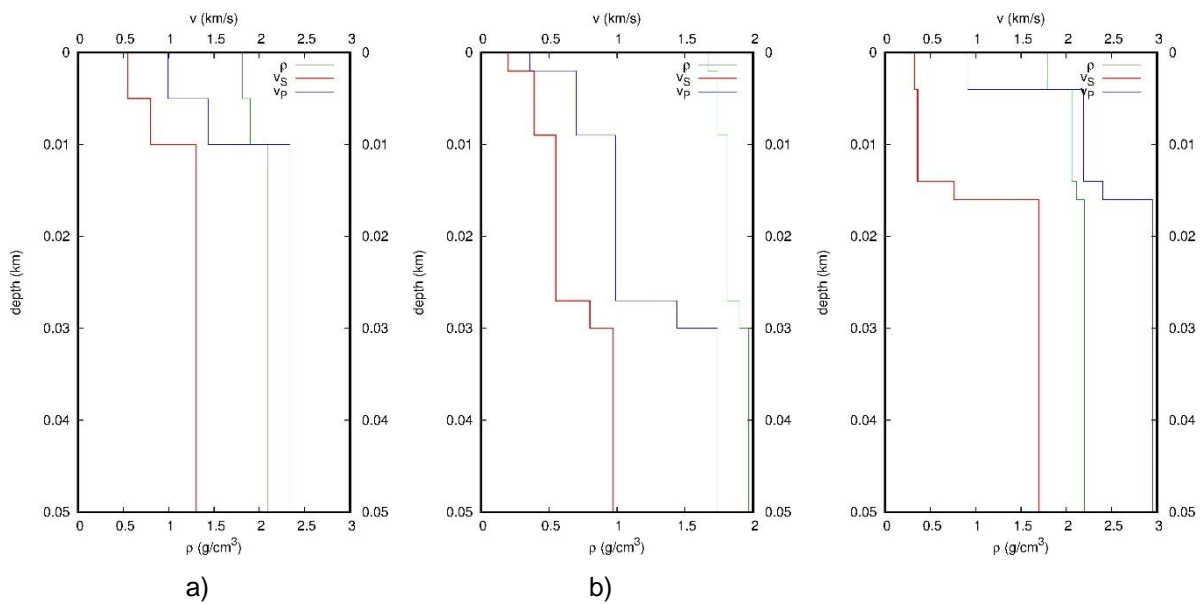


Figure 11: Example of shallow structures adopted for ITIS120: a) soil type A b) soil type B c) soil type C

### 3.3. Comparison of simulated data with GMPEs

To confirm the quality of the simulations, spectral accelerations were compared with the empirical predictions obtained from Bindi et al. (2011). Example of these comparisons are shown from Figure 12 to Figure 20 for different magnitudes and vibration periods. Left figures show the comparison with GMPE predictions whereas right figures show the standardized residuals distributions. Overall, even if the simulated cases do not include all range of cases that may be included in the GMPEs dataset definition (mainly different soil profiles and focal mechanisms), the comparisons show good agreement and residuals follow a normal distribution.

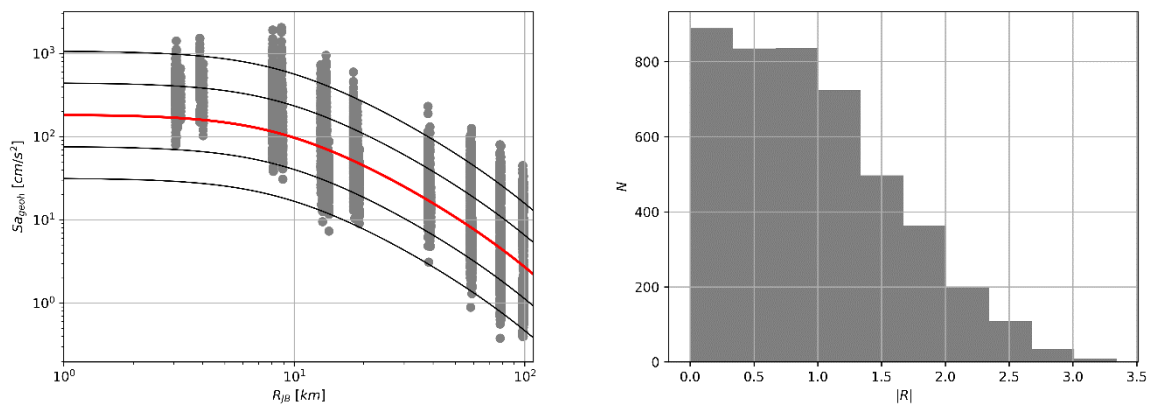


Figure 12: Comparisons of simulated spectral accelerations with GMPE: Mw = 5, T=0.2s; soil=A

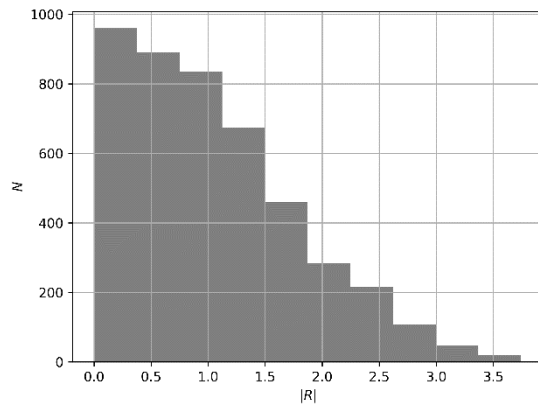
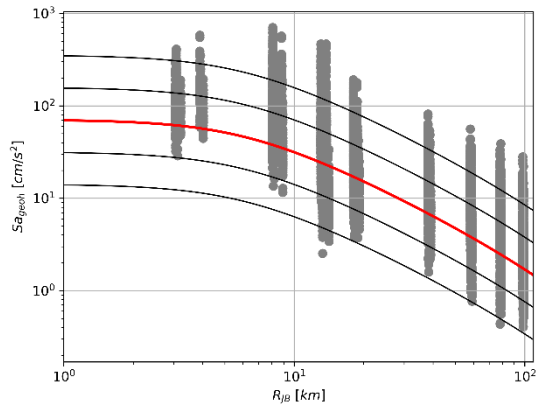


Figure 13: Comparisons of simulated spectral accelerations with GMPE: Mw = 5, T=0.5s; soil=A

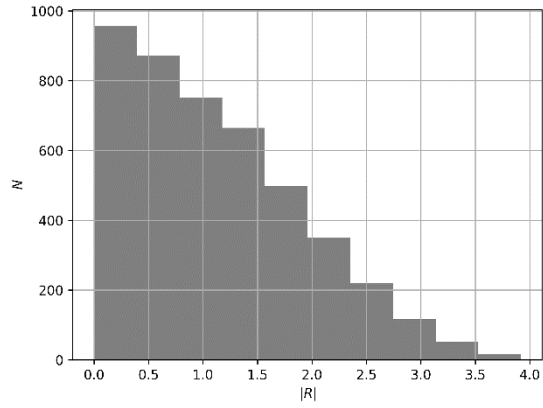
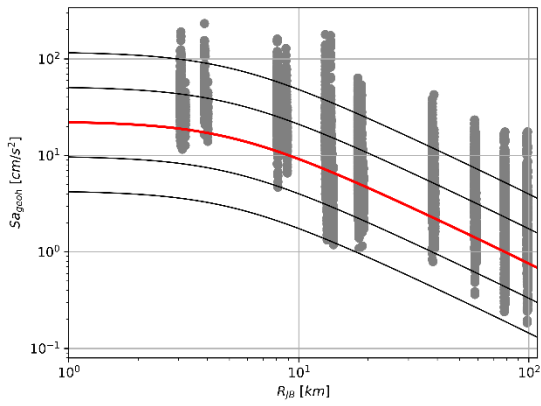


Figure 14: Comparisons of simulated spectral accelerations with GMPE: Mw = 5, T=1s; soil=A

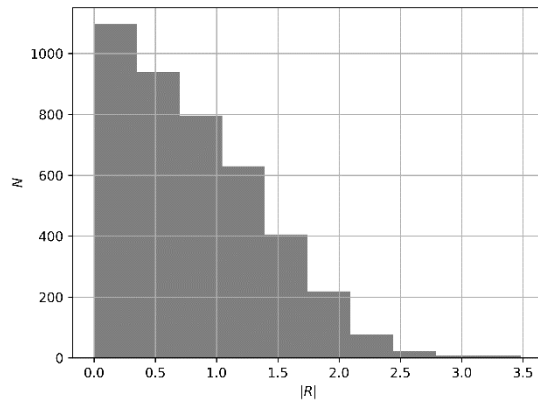
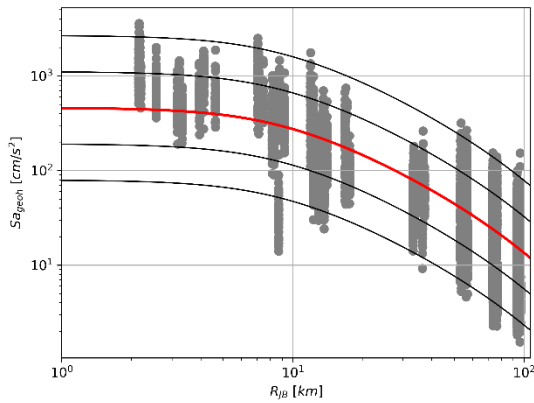


Figure 15: Comparisons of simulated spectral accelerations with GMPE: Mw = 6, T=0.2s; soil=A



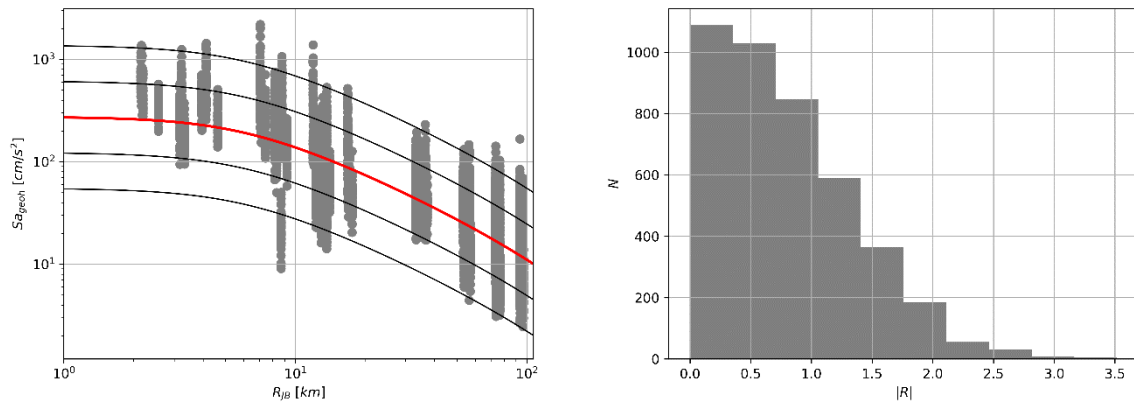


Figure 16: Comparisons of simulated spectral accelerations with GMPE: Mw = 6, T=0.5s; soil=A

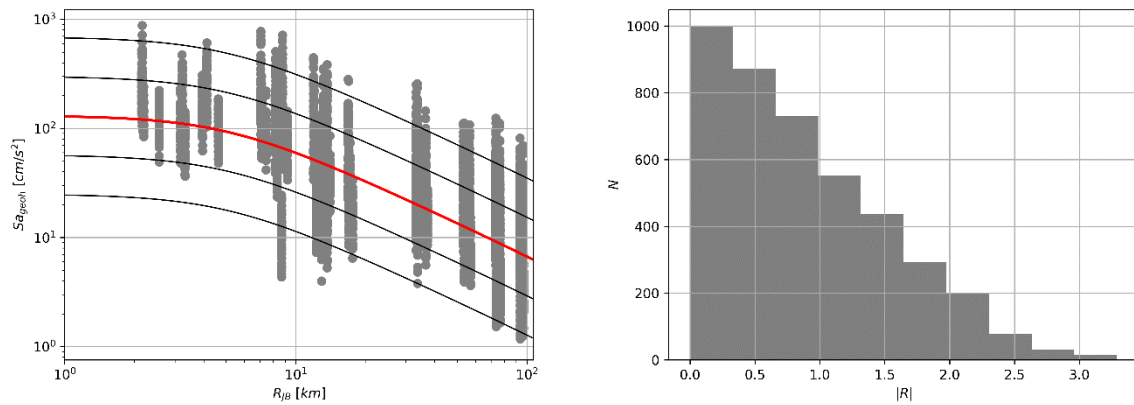


Figure 17: Comparisons of simulated spectral accelerations with GMPE: Mw = 6, T=1s; soil=A

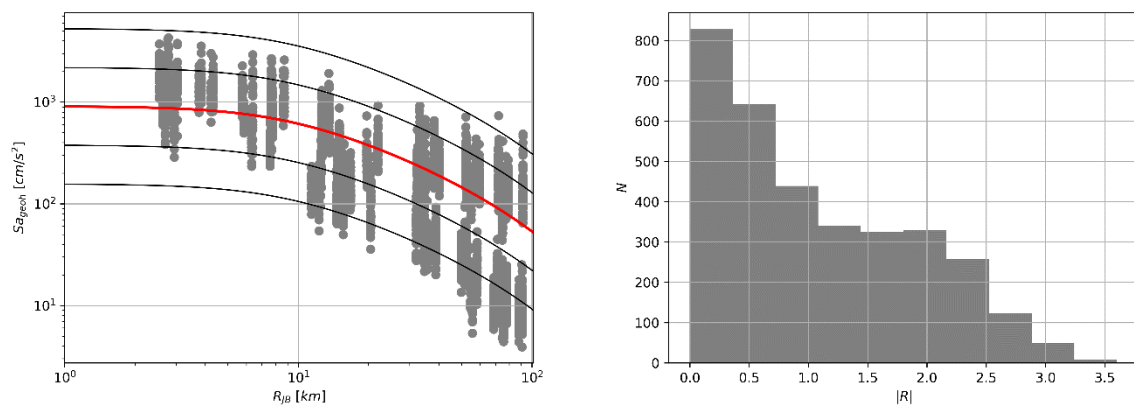


Figure 18: Comparisons of simulated spectral accelerations with GMPE: Mw = 7, T=0.2s; soil=A

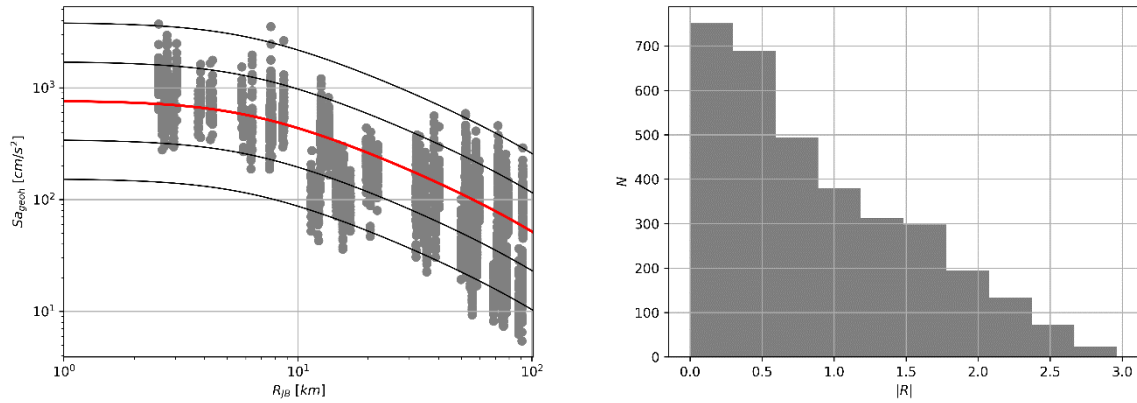


Figure 19: Comparisons of simulated spectral accelerations with GMPE: Mw = 7, T=0.5s; soil=A

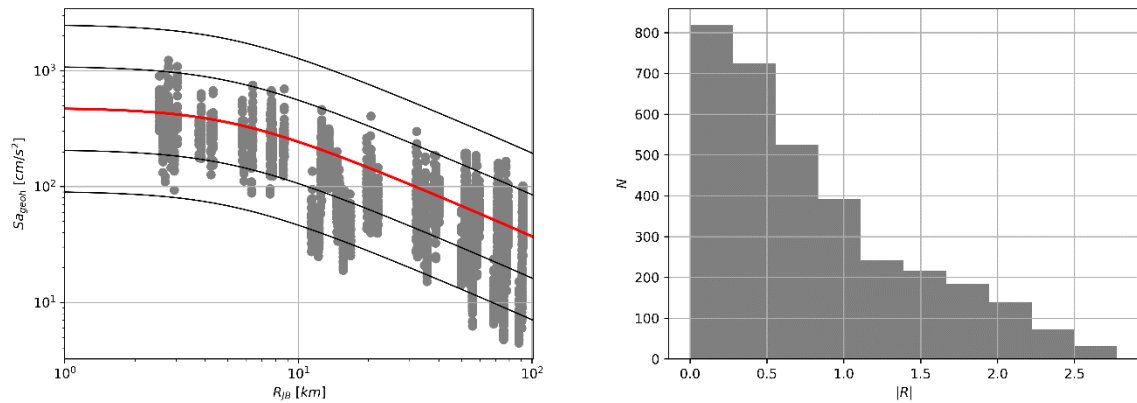


Figure 20: Comparisons of simulated spectral accelerations with GMPE: Mw = 7, T=1s; soil=A

### 3.4. Intensity assignment

The final scope of this work is to assign an “instrumental” macroseismic intensity to the simulations in order to group the simulated accelerograms in damage consistent bins. The idea is that signals leading to the same macroseismic intensity have the same damaging potential. According to Fasan (2020), the way EMS is assigned on field can be simulated numerically using non-linear time-history analysis (NLTHA) and modelling the behaviour of buildings of different vulnerability classes. Different building typology and vulnerability classes included in the EMS have been modelled using 141 equivalent non-linear SDOF. The characteristics of these SDOFs (yielding force  $F_y$ , displacement  $\delta_y$  and ductility  $\mu$ ) are extracted from Lagomarsino and Giovinazzi (2006) who proposed these values to develop a mechanical damage model in the framework of the RISK-EU project (Mouroux and Brun 2006) and are reported in APPENDIX 1. A bilinear non-degrading backbone with peak-oriented reloading stiffness was adopted as hysteretic behaviour. SDOF were modelled with OpenSEES using the modified peak oriented Ibarra-Medina-Krawinkler (IMK) hysteretic model (Ibarra et al. 2005). This hysteretic rule is able to account for the elongation of the structural period during a seismic event due to damage accumulation and it is therefore suited for the purposes of this study.

Based on Fasan (2020), the more suitable relation to be used to assign an “instrumental” macroseismic intensity is:

	$I_{EMS} = 6.012\mu_{kin,avg}^{0.133}$	(1)
--	--	-----

Where  $\mu_{kin,avg}$  represents the average kinematic ductility reached by the 141 different non-linear SDOF systems representing different buildings and vulnerability classes:

	$\mu_{kin,avg} = \frac{\sum_{i=1}^N \frac{\delta_{max,i}}{\delta_{y,i}}}{N}$	(2)
--	--	-----

$N = 141$  represents the number of SDOF systems used to describe the EMS building typologies.

$\delta_{max,i}$  is the maximum displacement reached by SDOF  $i$

$\delta_{min,i}$  is the minimum displacement reached by SDOF  $i$

$\delta_{y,i}$  is the yielding displacement of SDOF  $i$  (see Table 4 to Table 8)

$F_{y,i}$  is the yielding force of SDOF  $i$  (see Table 4 to Table 8)

This average kinematic ductility can predict  $I_{EMS}$  with a standard deviation of  $\sigma_{I_{EMS}} = 0.8$  that is comparable with standard deviations of commonly used linear GMPs. The standard deviation of  $\ln(I_{EMS})$  is  $\sigma_{\ln(I_{EMS})} = 0.140$ . Mean kinematic ductility can also be thought as a simplified numerical assessment of the mean damage on buildings of different vulnerabilities and strengths. Hence accelerograms showing the same macroseismic intensity (evaluated through the proposed equation) possess the same damaging potential. The European Macroseismic Intensity is used as a proxy to link this damage potential with real damage observations. Equation (1) is based on data gathered essentially for the Italian region. However, since the EMS vulnerability model is based on the European building stock and the selected correlation is based on structural demand and not on seismological parameters (such as magnitude-distance etc.) it is believed that the results can be applied also outside Italy. As shown in Figure 21 the proposed relation is well-tuned for intermediate intensity (that are the main focus of the work) whereas it loses power for high and low intensities. This is a problem related to huge uncertainties included in the relation definition and linked with: spatial ground motion variability, vulnerability of the building stock, subjectivity in the intensity assignment on the field. This problem is common to all relations available in literature between macroseismic intensity and other ground motion parameters. The relation here proposed is the outcome of hundreds of tests on different hypothesis and documented in (Fasan 2020).

Equation (1) can be transformed in a linear relation in the natural bi-logarithmic space:

	$\ln(I) = \ln(a) + b \ln(IM)$	(3)
--	-------------------------------	-----

Where  $I$  represents the macroseismic intensity,  $a=6.012$  the constant coefficient and  $b=0.133$  the exponent of Equation (1). The intensity measure  $IM$  is represented by the average kinematic ductility  $\mu_{kin,avg}$ . Using such form allows to apply standard methods used in structural analysis to develop fragility functions (Zentner et al. 2017; Bakalis and Vamvatsikos 2018) and therefore it is possible to evaluate the probability that the macroseismic intensity is higher or equal to a specific value given the occurrence of an intensity measure using the following relations (Figure 21):

	$P[I \geq i   IM] = 1 - \Phi \left( \frac{\ln(i) - \ln(a) - b \ln(IM)}{\sigma_{\ln I}} \right)$	(4)
--	---	-----

Where  $\Phi$  is the standard normal cumulative distribution function. These relations imply that residuals are normally distributed around the mean value (so given a macroseismic intensity ground motion parameters are log-normally distributed and the other way around) and that this dispersion is constant. Such hypotheses are at the base of a good regression model and are checked in Fasan (2020).

From equation (4) it is possible to evaluate the probability of experiencing a specific macroseismic intensity  $I$  given a signal with a specific intensity measure (in this case  $\mu_{kin,avg}$  as defined in (2)):

$$P[I = i|IM] = P[I \geq i|IM] - P[I \geq i + 1|IM] \quad (5)$$

and the average “instrumental” macroseismic intensity is finally evaluated as the central value applying the total probability theorem:

$$I_{EMS,avg} = \sum_{i=1}^{12} I_i \cdot P[I = i|IM] \quad (6)$$

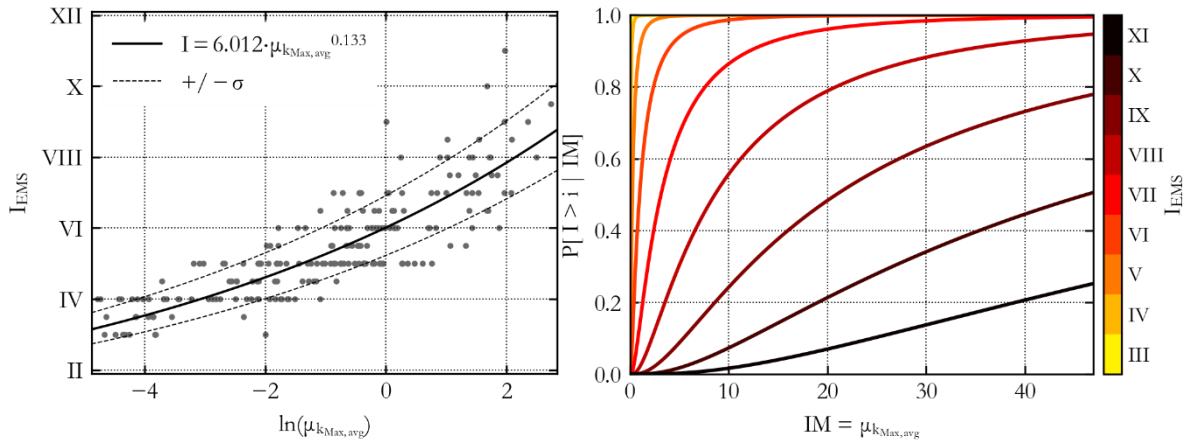


**Figure 21: Kinematic ductility  $\mu_{max}$  regression line (right) and “fragility” functions (left)**

As an example of the proposed procedure let us consider two events extracted from the simulations described in Section 3.2. The selected events correspond to two different realizations of the fault rupture process (R1 and R5) for a magnitude 7 recorded on soil A1 at a distance of 10 km from the fault centre along the direction corresponding to an angle of  $240^\circ$  from the horizontal direction. Ground motion accelerations for north-south (HNS) and east-west (HEW) component are shown in Figure 22 whereas the two different slip distributions on the fault plane are shown in Figure 23.

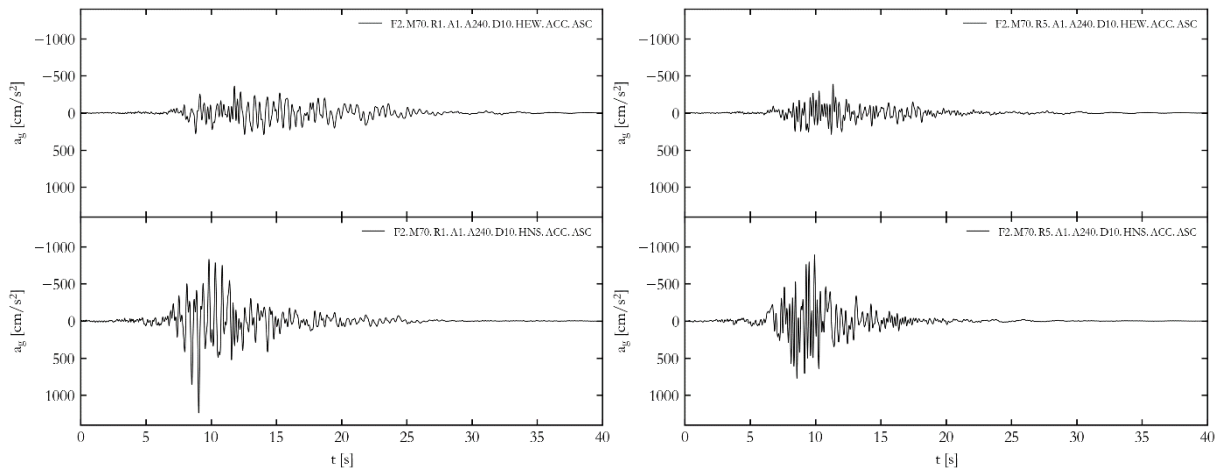


**Figure 22: Simulated ground motions for two different events having: Fault = F2 (ITIS129), Mw=7, D=10km,  $\alpha=240$ , R = 1(left) and 5 (right).**

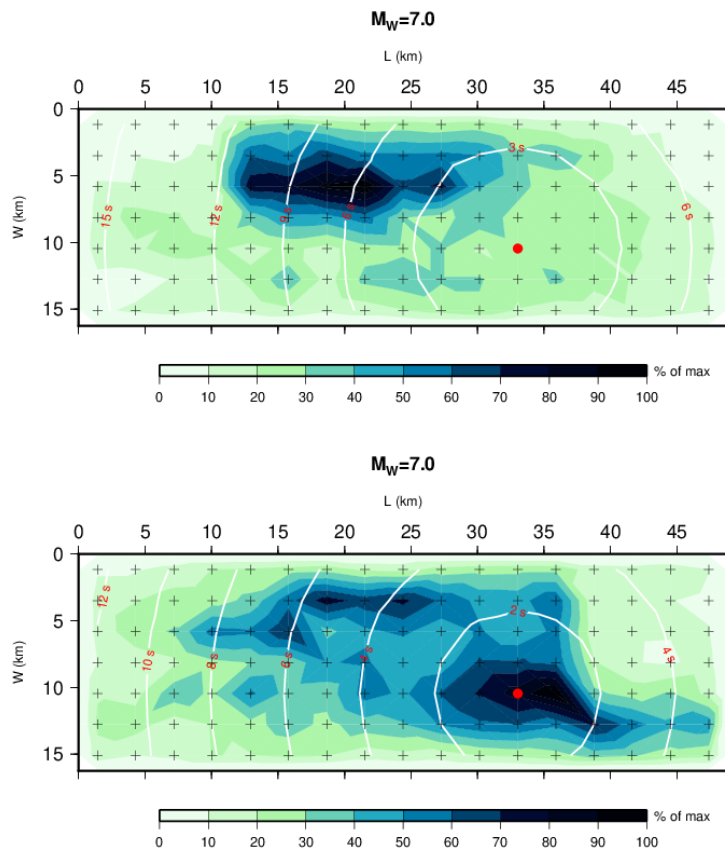


**Figure 23: realization R1 (up) and R5 (down) of the rupture process for the selected events. The darker areas correspond to a high slip on the fault while the red dot shows the nucleation point of the rupture. The white isochrones describe the time evolution of the rupture process.**

After running the 141 NLTHA with the selected accelerograms, the first shows an average kinematic ductility demand of about 28 whereas the second of about 15. These results lead to the probability distributions shown in Figure 24 and to a final average macroseismic intensity of IX (nine) for the first event and VIII (eight) for the second event.

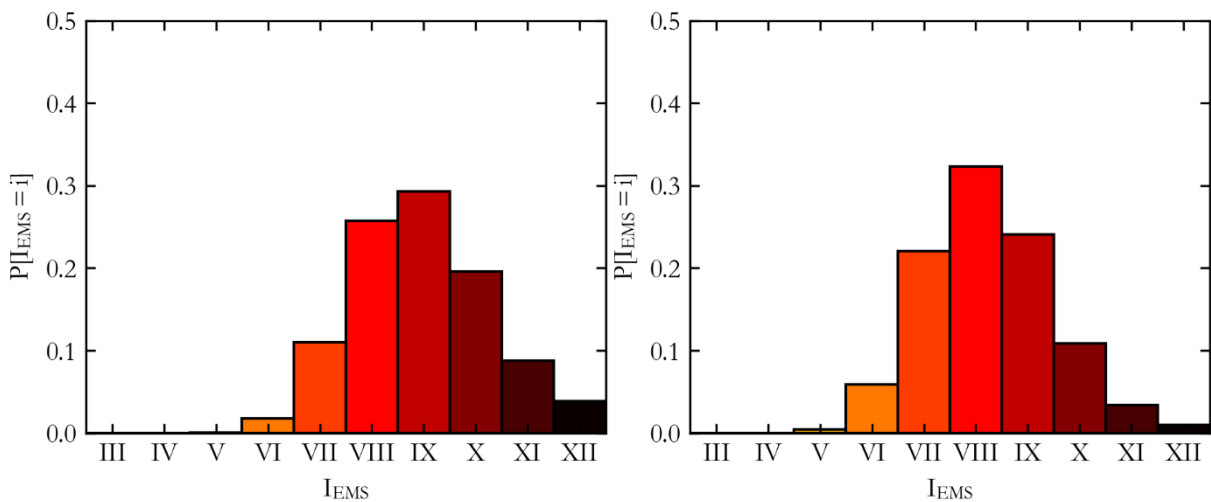


**Figure 24: Macroseismic intensity probability distribution for events 1 (left) and 2 (right)**

## 4. Conclusions

In the present work a database of natural accelerograms is constructed matching available ground motion and macroseismic data. In order to increment the availability of accelerograms a database of 115200 physics-based simulated events is computed. The events are represented by three components broadband accelerograms and account for different sources of variability. Using a relation proposed in the first deliverable of this task, an average instrumental macroseismic intensity has been assigned to each simulated triplet of accelerograms. The relation investigates the mean kinematic ductility demand of the accelerograms on buildings having different strength and vibrational characteristics and links it with the macroseismic intensity. The value assigned to each accelerogram represents the central values and considers the expected variability due to the uncertainties related to the ability of the kinematic ductility to predict the macroseismic intensity. The macroseismic intensity is therefore used as a proxy to explain the damaging potential of a signal and is used to separate accelerograms in damage-consistent bins. The magnitude-distance distribution of the final simulated database along with the intensity distribution is shown in Figure 25. Magnitude ranges from 4.5 to 8 and epicentral distances from 0 to 120 kilometres (the simulated epicentre has been taken as the projection of the nucleation point). Compared to the database compiled based on records, the simulated one has a much better coverage of magnitudes and distances and thus, represents an excellent basis for practical application. The macroseismic intensities range from II to XI.

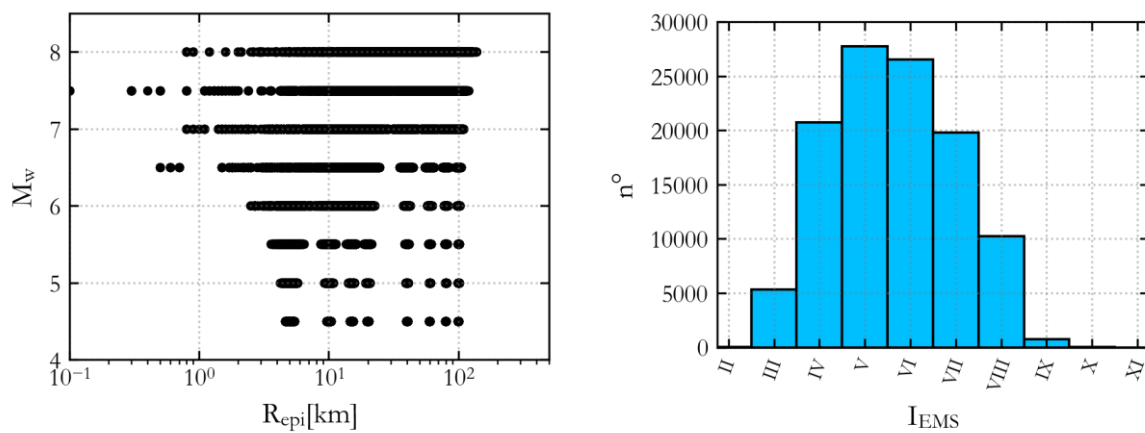


**Figure 25: Magnitude vs Epicentral distance of the records included in the simulated dataset (left) and Distribution intensity degrees (right)**

## 5. Bibliography

- Aki K (1967) Scaling law of seismic spectrum. *Journal of Geophysical Research* 72:1217–1231. doi: 10.1029/JZ072i004p01217
- Azzaro R, Barbano MS, D'Amico S, et al (2011) The L'Aquila 2009 earthquake: An application of the European Macroseismic Scale to the damage survey in the epicentral area. *Bollettino di Geofisica Teorica ed Applicata* 52:561–581. doi: 10.4430/bgta0012
- Bakalis K, Vamvatsikos D (2018) Seismic Fragility Functions via Nonlinear Response History Analysis. *Journal of Structural Engineering (United States)* 144:1–15. doi: 10.1061/(ASCE)ST.1943-541X.0002141
- Bindi D, Pacor F, Luzi L, et al (2011) Ground motion prediction equations derived from the Italian strong motion database. *Bulletin of Earthquake Engineering* 9:1899–1920. doi: 10.1007/s10518-011-9313-z
- Brandmayr E, Raykova RB, Zuri M, et al (2010) The lithosphere in Italy: structure and seismicity. *Journal of the Virtual Explorer* 36:. doi: 10.3809/jvirtex.2010.00224
- Cornell BYCA (1968) Engineering Seismic Risk Analysis. *Bulletin of the Seismological Society of America* 58:1583–1606
- DISS Working Group (2018) Database of Individual Seismogenic Sources (DISS), Version 3.2.1: A compilation of potential sources for earthquakes larger than M 5.5 in Italy and surrounding areas. <http://diss.rm.ingv.it/diss/>
- Fasan M (2020) Relate macroseismic intensity (EMS-98) to ground-motion parameters. SIGMA2 project report
- Fasan M (2017) Advanced seismological and engineering analysis for structural seismic design. University of Trieste
- Fasan M, Magrin A, Amadio C, et al (2016) A seismological and engineering perspective on the 2016 Central Italy earthquakes. *International Journal of Earthquake and Impact Engineering* 1:395–420. doi: 10.1504/IJEIE.2016.10004076
- Graziani L, Tertulliani A, Maramai A, et al (2017) The 7 and 11 May 1984 earthquakes in Abruzzo-Latium (Central Italy): reappraisal of the existing macroseismic datasets according to the EMS98. *Journal of Seismology* 21:1219–1227. doi: 10.1007/s10950-017-9663-3
- Grünthal G (1998) European Macroseismic Scale 1998
- Gusev AA (2011) Broadband Kinematic Stochastic Simulation of an Earthquake Source: a Refined Procedure for Application in Seismic Hazard Studies. *Pure and Applied Geophysics* 168:155–200. doi: 10.1007/s00024-010-0156-3
- Haskell NA (1964) Total energy and energy spectral density of elastic wave radiation from propagating faults. *Bulletin of the Seismological Society of America* 54:1811–1841
- Hassan HM, Fasan M, Sayed MA, et al (2020) Site-specific ground motion modeling for a historical Cairo site as a step towards computation of seismic input at cultural heritage sites. *Engineering Geology* 268:105524. doi: 10.1016/j.enggeo.2020.105524
- Heaton TH (1990) Evidence for and implications of self-healing pulses of slip in earthquake rupture. *Physics of the Earth and Planetary Interiors* 64:1–20. doi: 10.1016/0031-9201(90)90002-F
- Ibarra LF, Medina RA, Krawinkler H (2005) Hysteretic models that incorporate strength and stiffness deterioration. *Earthquake Engineering & Structural Dynamics* 34:1489–1511. doi: 10.1002/eqe.495
- Kanamori H, Anderson DL (1975) Theoretical basis of some empirical relations in seismology. *Bulletin of the Seismological Society of America* 65:1073–1095
- Klügel J-U, Stäuble-Akçay S (2018) Towards damage-consistent performance-based design of critical infrastructures. *International Journal of Computational Methods and Experimental Measurements* 6:933–943. doi: 10.2495/cmeme-v6-n5-933-943

- Lagamarsino S, Giovinazzi S (2006) Macroseismic and mechanical models for the vulnerability and damage assessment of current buildings. *Bulletin of Earthquake Engineering* 4:415–443. doi: 10.1007/s10518-006-9024-z
- Lanzano G, Sgobba S, Luzi L, et al (2019) The pan-European Engineering Strong Motion (ESM) flatfile: compilation criteria and data statistics. *Bulletin of Earthquake Engineering* 17:561–582. doi: 10.1007/s10518-018-0480-z
- Locati M, Camassi R, Rovida A, et al (2016) Database Macrosismico Italiano , versione DBMI15
- Magrin A (2012) Multi-scale seismic hazard scenarios. University of Trieste
- Magrin A, Gusev AA, Romanelli F, et al (2016) Broadband NDSHA computations and earthquake ground motion observations for the Italian territory. *International Journal of Earthquake and Impact Engineering* 1:28. doi: 10.1504/IJEIE.2016.10000979
- Mouroux P, Brun B Le (2006) Presentation of RISK-UE Project. *Bulletin of Earthquake Engineering* 4:323–339. doi: 10.1007/s10518-006-9020-3
- Musson RMW, Grünthal G, Stucchi M (2010) The comparison of macroseismic intensity scales. *Journal of Seismology* 14:413–428. doi: 10.1007/s10950-009-9172-0
- Panza GF (2001) SEISMIC WAVE PROPAGATION IN LATERALLY HETEROGENEOUS ANELASTIC MEDIA: THEORY AND APPLICATIONS TO SEISMIC ZONATION Giuliano. *Advances in Geophysics* 43:1–95
- Panza GF, Mura C La, Peresan A, et al (2012) Seismic Hazard Scenarios as Preventive Tools for a Disaster Resilient Society. pp 93–165
- Paolucci R, Gatti F, Infantino M, et al (2018) Broadband Ground Motions from 3D Physics-Based Numerical Simulations Using Artificial Neural Networks. *Bulletin of the Seismological Society of America* 108:1272–1286. doi: 10.1785/0120170293
- Pavlov VM (2009) Matrix impedance in the problem of the calculation of synthetic seismograms for a layered-homogeneous isotropic elastic medium. *Izvestiya, Physics of the Solid Earth* 45:850–860. doi: 10.1134/S1069351309100036
- Rossi A, Tertulliani A, Azzaro R, et al (2019) The 2016–2017 earthquake sequence in Central Italy: macroseismic survey and damage scenario through the EMS-98 intensity assessment. *Bulletin of Earthquake Engineering* 17:2407–2431. doi: 10.1007/s10518-019-00556-w
- Tertulliani A, Arcoraci L, Berardi M, et al (2012) The Emilia 2012 sequence: A macroseismic survey. *Annals of Geophysics* 55:679–687. doi: 10.4401/ag-6140
- Tertulliani A, Cčić I, Meurers R, et al (2018) The 6 May 1976 Friuli earthquake: Re-evaluating and consolidating transnational macroseismic data. *Bollettino di Geofisica Teorica ed Applicata* 59:417–444. doi: 10.4430/bgta0234
- Wells DL, Coppersmith KJ (1994) New empirical relationships among magnitude, rupture length, rupture width, rupture area, and surface displacement. *Bulletin - Seismological Society of America* 84:974–1002
- Zentner I, Gündel M, Bonfils N (2017) Fragility analysis methods: Review of existing approaches and application. *Nuclear Engineering and Design* 323:245–258. doi: 10.1016/j.nucengdes.2016.12.021



## APPENDIX 1 Characteristics of the modelled SDOF systems

Table 4: Masonry building typologies: defining parameters.

Building Typology	T [s]	Fy [g]	$\delta y$ [m]	$\delta u$ [m]
M1_L	0.211	0.168	0.0019	0.0089
M1_M	0.355	0.133	0.0042	0.0135
M1.w_L	0.211	0.178	0.0020	0.0094
M1.w_M	0.355	0.141	0.0044	0.0143
M1.v_L	0.211	0.132	0.0015	0.0070
M1.v_M	0.355	0.105	0.0033	0.0107
M2_L	0.268	0.146	0.0026	0.0104
M2.w_L	0.268	0.155	0.0028	0.0111
M2.v_L	0.268	0.116	0.0021	0.0082
M3_L	0.192	0.248	0.0023	0.0117
M3_M	0.322	0.196	0.0051	0.0176
M3_H	0.437	0.142	0.0067	0.0202
M3.w_L	0.192	0.263	0.0024	0.0124
M3.w_M	0.322	0.208	0.0054	0.0187
M3.w_H	0.437	0.151	0.0071	0.0214
M3.v_L	0.192	0.196	0.0018	0.0093
M3.v_M	0.322	0.155	0.0040	0.0140
M3.v_H	0.437	0.112	0.0053	0.0160
M3.sm_L	0.192	0.296	0.0027	0.0140
M3.sm_M	0.322	0.234	0.0060	0.0210
M3.sm_H	0.437	0.170	0.0080	0.0241
M4_L	0.173	0.358	0.0026	0.0149
M4_M	0.290	0.283	0.0059	0.0222
M4_H	0.393	0.223	0.0086	0.0260
M4.w_L	0.173	0.379	0.0028	0.0158
M4.w_M	0.290	0.300	0.0063	0.0235
M4.w_H	0.393	0.237	0.0091	0.0276
M4.v_L	0.173	0.283	0.0021	0.0118
M4.v_M	0.290	0.223	0.0047	0.0176
M4.v_H	0.393	0.177	0.0068	0.0206
M5_L	0.173	0.263	0.0019	0.0110
M5_M	0.290	0.208	0.0044	0.0164
M5_H	0.393	0.165	0.0063	0.0192
M5.w_L	0.201	0.279	0.0028	0.0140
M5.w_M	0.338	0.221	0.0063	0.0211
M5.w_H	0.459	0.152	0.0080	0.0239
M5.v_L	0.192	0.208	0.0019	0.0098
M5.v_M	0.322	0.165	0.0043	0.0148
M5.v_H	0.437	0.119	0.0057	0.0170
M5.sm_L	0.192	0.314	0.0029	0.0148

M5.sm_M	0.322	0.248	0.0064	0.0223
M5.sm_H	0.437	0.180	0.0085	0.0256
M6_L-PC	0.211	0.324	0.0036	0.0171
M6_M-PC	0.355	0.256	0.0080	0.0260
M6_H-PC	0.481	0.168	0.0097	0.0290
M6_L-MC	0.211	0.358	0.0040	0.0236
M6_M-MC	0.355	0.283	0.0088	0.0350
M6_H-MC	0.481	0.186	0.0107	0.0387
M7_L	0.153	0.508	0.0030	0.0233
M7_M	0.258	0.401	0.0066	0.0336
M7_H	0.350	0.317	0.0096	0.0386

**Table 5: Non-designed reinforced concrete buildings: defining parameters**

Building Typology	T [s]	Fy [g]	$\delta y$ [m]	$\delta u$ [m]
RC1_L	0.539	0.207	0.0150	0.0451
RC1_M	0.854	0.124	0.0224	0.0674
RC1_H	1.304	0.072	0.0304	0.0915
RC2_L	0.539	0.278	0.0201	0.0606
RC2_M	0.854	0.166	0.0300	0.0904
RC2_H	1.304	0.097	0.0407	0.1227
RC3_L	0.539	0.240	0.0174	0.0523
RC3_M	0.854	0.143	0.0259	0.0781
RC3_H	1.304	0.083	0.0352	0.1060

**Table 6: DCL reinforced concrete buildings: defining parameters**

Building Typology	T [s]	Fy [g]	$\delta y$ [m]	$\delta u$ [m]
L_RC1-III_L	0.437	0.227	0.0108	0.0324
L_RC1-III_M	0.642	0.164	0.0168	0.0504
L_RC1-III_H	0.913	0.115	0.0239	0.0717
L_RC1-II_L	0.437	0.363	0.0173	0.0518
L_RC1-II_M	0.642	0.263	0.0269	0.0806
L_RC1-II_H	0.913	0.185	0.0382	0.1147
L_RC1-I_L	0.437	0.502	0.0239	0.0716
L_RC1-I_M	0.642	0.363	0.0371	0.1114
L_RC1-I_H	0.913	0.255	0.0528	0.1584
L_RC2-III_L	0.437	0.305	0.0145	0.0434
L_RC2-III_M	0.642	0.220	0.0225	0.0676
L_RC2-III_H	0.913	0.155	0.0321	0.0962
L_RC2-II_L	0.437	0.487	0.0232	0.0695
L_RC2-II_M	0.642	0.352	0.0361	0.1081
L_RC2-II_H	0.913	0.248	0.0513	0.1538
L_RC2-I_L	0.437	0.673	0.0320	0.0960

L_RC2-I_M	0.642	0.487	0.0498	0.1494
L_RC2-I_H	0.913	0.342	0.0709	0.2125
L_RC3-III_L	0.437	0.263	0.0125	0.0375
L_RC3-III_M	0.642	0.190	0.0195	0.0584
L_RC3-III_H	0.913	0.134	0.0277	0.0830
L_RC3-II_L	0.437	0.421	0.0200	0.0600
L_RC3-II_M	0.642	0.304	0.0311	0.0934
L_RC3-II_H	0.913	0.214	0.0443	0.1328
L_RC3-I_L	0.437	0.581	0.0276	0.0829
L_RC3-I_M	0.642	0.420	0.0430	0.1290
L_RC3-I_H	0.913	0.295	0.0612	0.1835

**Table 7: DCM reinforced concrete buildings: defining parameters**

Building Typology	T [s]	Fy [g]	$\delta y$ [m]	$\delta u$ [m]
M_RC1-III_L	0.437	0.266	0.0127	0.0459
M_RC1-III_M	0.642	0.176	0.0180	0.0742
M_RC1-III_H	0.913	0.117	0.0242	0.0995
M_RC1-II_L	0.437	0.426	0.0203	0.0735
M_RC1-II_M	0.642	0.282	0.0288	0.1187
M_RC1-II_H	0.913	0.187	0.0387	0.1592
M_RC1-I_L	0.437	0.589	0.0280	0.1015
M_RC1-I_M	0.642	0.389	0.0398	0.1639
M_RC1-I_H	0.913	0.258	0.0534	0.2199
M_RC2-III_L	0.437	0.391	0.0186	0.0594
M_RC2-III_M	0.642	0.258	0.0264	0.0959
M_RC2-III_H	0.913	0.171	0.0355	0.1286
M_RC2-II_L	0.437	0.625	0.0297	0.0950
M_RC2-II_M	0.642	0.413	0.0423	0.1534
M_RC2-II_H	0.913	0.274	0.0568	0.2058
M_RC2-I_L	0.437	0.864	0.0411	0.1312
M_RC2-I_M	0.642	0.571	0.0584	0.2119
M_RC2-I_H	0.913	0.379	0.0784	0.2842
M_RC3-III_L	0.437	0.337	0.0160	0.0513
M_RC3-III_M	0.642	0.223	0.0228	0.0828
M_RC3-III_H	0.913	0.148	0.0306	0.1110
M_RC3-II_L	0.437	0.540	0.0257	0.0820
M_RC3-II_M	0.642	0.357	0.0365	0.1324
M_RC3-II_H	0.913	0.237	0.0490	0.1776
M_RC3-I_L	0.437	0.746	0.0355	0.1133
M_RC3-I_M	0.642	0.493	0.0505	0.1829
M_RC3-I_H	0.913	0.327	0.0677	0.2454

**Table 8: DCH reinforced concrete buildings: defining parameters**

Building Typology	T [s]	Fy [g]	$\delta y$ [m]	$\delta u$ [m]
H_RC1-III_L	0.437	0.251	0.0119	0.0557
H_RC1-III_M	0.642	0.141	0.0144	0.0814
H_RC1-III_H	0.913	0.093	0.0193	0.1092
H_RC1-II_L	0.437	0.401	0.0191	0.0890
H_RC1-II_M	0.642	0.225	0.0231	0.1302
H_RC1-II_H	0.913	0.149	0.0309	0.1747
H_RC1-I_L	0.437	0.554	0.0263	0.1230
H_RC1-I_M	0.642	0.311	0.0319	0.1799
H_RC1-I_H	0.913	0.206	0.0427	0.2413
H_RC2-III_L	0.437	0.368	0.0175	0.0719
H_RC2-III_M	0.642	0.207	0.0211	0.1052
H_RC2-III_H	0.913	0.137	0.0284	0.1411
H_RC2-II_L	0.437	0.588	0.0280	0.1151
H_RC2-II_M	0.642	0.331	0.0338	0.1683
H_RC2-II_H	0.913	0.219	0.0454	0.2258
H_RC2-I_L	0.437	0.813	0.0386	0.1590
H_RC2-I_M	0.642	0.457	0.0467	0.2325
H_RC2-I_H	0.913	0.303	0.0627	0.3119
H_RC3-III_L	0.437	0.317	0.0151	0.0621
H_RC3-III_M	0.642	0.178	0.0183	0.0908
H_RC3-III_H	0.913	0.118	0.0245	0.1218
H_RC3-II_L	0.437	0.508	0.0242	0.0994
H_RC3-II_M	0.642	0.286	0.0292	0.1453
H_RC3-II_H	0.913	0.189	0.0392	0.1949
H_RC3-I_L	0.437	0.702	0.0334	0.1373
H_RC3-I_M	0.642	0.394	0.0404	0.2008
H_RC3-I_H	0.913	0.261	0.0541	0.2693

## APPENDIX 2 File name description for the physics-based database

The files name with \*.ASC extension are formed using the following scheme:

Fault.Magnitude.Realization.Soil.Angle.Distance.component.file type.ASC

The codes are:

- Faults (4): with relative crustal models
  - F1 ITIS131 - Paganica
  - F2 ITIS120 - Gemona South
  - F3 ITIS107 - Mirandola
  - F4 ITIS052 - San Giuliano di Puglia
- Angles (6):
  - A0, A60, A120, A180, A240, A300
- Local soil (15 – 5 five profiles for each of the categories A, B and C):
  - A1, A2, ..., C4, C5
- Realization (5 realizations):
  - R1, ..., R5
- Magnitude (8, from 4.5 to 8 at 0.5 step):
  - M45, M50, ..., M75, M80
- Distance: (8):
  - D5, D10, D15, D20, D40, D60, D80, D100
- Components (3):
  - HNS – North south
  - HEW – Est West
  - VZZ – Vertical
- Type of file
  - ACC accelerations;
  - SA Spectral accelerations

Example:

- Fault ITIS131
- Magnitude 5.5
- Realization 3
- Local soil B3
- Receiver angle 0°
- Distance from fault centre 15 km
- Component Est West
- Accelerations

F1.M55.R3.B3. A0.D15.HEW.ACC.ASC

### APPENDIX 3 Files header

The header of the file contains the same 65 lines contained in the files coming from the European Strong Motion database. An example (with descriptions) is as follows:

```

EVENT_NAME:          F2.M70.R1.A1.A240.D10 (Fault.Magnitude.Realization.Soil.Angle.Distance)
EVENT_ID:
EVENT_DATE_YYYYMMDD:      20201027 (date of computation)
EVENT_TIME_HHMMSS:        16478 (time of computation)
EVENT_LATITUDE_DEGREE:    46.3210 (latitude of the nucleation point)
EVENT_LONGITUDE_DEGREE:   13.0619 (longitude of the nucleation point)
EVENT_DEPTH_KM:           7.2 (depth of the nucleation point)
HYPOCENTER_REFERENCE:     DIA_DMG_UniTS
MAGNITUDE_W:              7.0 (simulated magnitude)
MAGNITUDE_W_REFERENCE:   DIA_DMG_UniTS
MAGNITUDE_L:
MAGNITUDE_L_REFERENCE:
FOCAL_MECHANISM:         TF
                          The focal mechanisms used are:
                          NF (normal fault)
                          TF (trust fault)
                          SS (strike-slip)
                          DIA_DMG_UniTS

NETWORK:
STATION_CODE:            F2.A1.A240.D10 (Fault.Soil.Angle.Distance)
STATION_NAME:            F2.A1.A240.D10 (Fault.Soil.Angle.Distance)
STATION_LATITUDE_DEGREE: 46.199600 (latitude of the receiver)
STATION_LONGITUDE_DEGREE: 13.093200 (longitude of the receiver)
STATION_ELEVATION_M:
LOCATION:
SENSOR_DEPTH_M:          0.0
VS30_M/S:                1092 (Vs,30 of the local stratigraphy in m/s)
SITE_CLASSIFICATION_EC8:  A (EC8 soil class A, B or C)
EPICENTRAL_DISTANCE_KM:  13.7 (distance receiver – projection of the nucleation
point)
EARTHQUAKE_BACKAZIMUTH_DEGREE: 90.0
DATE_TIME_FIRST_SAMPLE_YYYYMMDD_HHMMSS:
DATE_TIME_FIRST_SAMPLE_PRECISION: seconds
SAMPLING_INTERVAL_S:     0.005000 (time step of signals used in computations)
NDATA:                    40000 (number of data)
DURATION_S:               200.000 (signal duration)
STREAM:                   HNS (signal component)
INSTRUMENT:               Physics-Based simulation
INSTRUMENT_ANALOG/DIGITAL: Physics-Based simulation
INSTRUMENTAL_FREQUENCY_HZ: 10 Hz (maximum frequency used in computations)
INSTRUMENTAL_DAMPING:
FULL_SCALE_G:
N_BIT_DIGITAL_CONVERTER:
PGA_CM/S^2:               1237.06 (pga in cm/s^2)
TIME_PGA_S:
BASELINE_CORRECTION:
FILTER_TYPE:
FILTER_ORDER:
LOW_CUT_FREQUENCY_HZ:
HIGH_CUT_FREQUENCY_HZ:
LATE/NORMAL_TRIGGERED:
DATABASE_VERSION:
HEADER_FORMAT:
DATA_TYPE:                ACC (accelerations)
PROCESSING:
  
```

DATA\_TIMESTAMP\_YYYYMMDD\_HHMMSS:

DATA\_LICENSE:

DATA\_CITATION:

DATA\_CREATOR:

ORIGINAL\_DATA\_MEDIATOR\_CITATION:

ORIGINAL\_DATA\_MEDIATOR:

ORIGINAL\_DATA\_CREATOR\_CITATION: DIA\_DMG\_UniTS (M. Fasan, M. Barnaba)

ORIGINAL\_DATA\_CREATOR: M. Fasan, M. Barnaba

USER1: European Macroseismic Intensity : lems = 9 (lems assessed as in this report)

USER2:

USER3:

USER4:

USER5: